Cadmium-Free $CuInS_2$/ZnS Quantum Dots for Sentinel Lymph Node Imaging with Reduced Toxicity

Thomas Pons,[†,*] Emilie Pic,[‡] Nicolas Lequeux,[§] Elsa Cassette,[†] Lina Bezdetnaya,[‡] François Guillemin,[‡] Frédéric Marchal,[‡] and Benoit Dubertret[†]

[†]Laboratoire Physique et Etude des Matériaux, CNRS UPR0005, ESPCI, 10, rue Vauquelin, 75005 Paris, France, [‡]Centre de Recherche en Automatique de Nancy, Nancy-University, CNRS, Centre Alexis Vautrin, avenue de Bourgogne, 54511 Vandoeuvre-lès-Nancy Cedex, France, and [§]Laboratoire de physico-chimie des Polymères et des Milieux Dispersés, CNRS UMR7615, ESPCI, 10, rue Vauquelin, 75005 Paris, France

ABSTRACT Semiconductor quantum dots (QDs) could significantly impact the performance of biomedical near-infrared (NIR) imaging by providing fluorescent probes that are brighter and more photostable than conventional organic dyes. However, the toxicity of the components of NIR emitting II—VI and IV—VI QDs that have been made so far (Cd, Hg, Te, Pb, *etc.*) has remained a major obstacle to the clinical use of QDs. Here, we present the synthesis of $CuInS_2$/ZnS core/shell QDs emitting in the NIR (~800 nm) with good quantum yield and stability even after transfer into water. We demonstrate the potential of these QDs by imaging two regional lymph nodes (LNs) *in vivo* in mice. We then compare the inflammatory response of the axillary LN induced by different doses of $CuInS_2$/ZnS and CdTeSe/CdZnS QDs and show a clear difference in acute local toxicity, the onset of inflammation only occurring at a 10 times more concentrated dose for $CuInS_2$/ZnS QDs than for their Cd-containing counterparts.

KEYWORDS: quantum dots · $CuInS_2$ · copper indium sulfide · near-infrared · *in vivo* · toxicity · lymph node

Semiconductor nanocrystals, or quantum dots (QDs), have attracted much attention over the past years as a novel class of material with unique electronic and optical properties.[1,2] They display high extinction coefficients, photoluminescence (PL) quantum yields (QYs), and photostability, and their narrow emission spectra can be tuned by size and composition. They have therefore become promising alternatives to organic chromophores in many applications as light absorbers or emitters, from photovoltaics and light emitting diodes to fluorescent probes for biological imaging.[3,4] In particular, QDs have the potential to significantly impact the performance of near-infrared fluorescence (NIR) imaging for biomedical research, diagnostics, and optically assisted surgery. Examples of biomedical applications of QDs include *in vivo* tumor detection,[5] cell tracking,[6] and detection of the sentinel lymph node, the status of which is a key prognostic factor for treatment of many types of cancer.[7,8] Unfortunately, QDs emitting in the NIR, the optimal spectral window for *in vivo* imaging, have been so far composed of toxic compounds (Cd, Pb, Hg, Te, As, *etc.*). Several groups have shown that *in vitro* toxicity of CdSe-based QDs strongly depends on the presence of a ZnS inorganic shell capable of slowing down the release of Cd^{2+} ions into the cellular environment and on the nature of the organic capping layer that is responsible for both the cellular distribution and the protection of the QD against oxidation.[9−16] In contrast, the *in vivo* toxicity of QDs has been much less studied. Of particular concern is the long-term sequestration of injected QDs in organs such as the liver[16−19] since it will eventually lead to a release of these toxic elements in the body. This represents a major obstacle to the clinical use of QDs and has motivated the development of Cd-free NIR QDs, based on III−V or I−III−VI_2 materials. However, so far, there has not been to our knowledge any demonstration that these materials were indeed less toxic than their CdSe or CdTe-based counterparts while being used for *in vivo* imaging with the same level of performance.

$CuInS_2$ is a I−III−VI_2 semiconductor with a direct band gap of 1.45 eV, corresponding to an 855 nm emission wavelength, and does not contain any toxic heavy metals. This material could therefore offer the opportunity to fulfill the potential of semiconductor QDs without the toxicity limitations encountered by II−VI QDs and provide PL emission ranging from the visible to the NIR. Several syntheses of QDs based on $CuInS_2$ or other I−III−VI_2 semiconductors have already been described;[20−27] however, most of the

*Address correspondence to thomas.pons@espci.fr.

Received for review October 15, 2009 and accepted March 31, 2010.

Published online April 13, 2010.
10.1021/nn901421v

© 2010 American Chemical Society

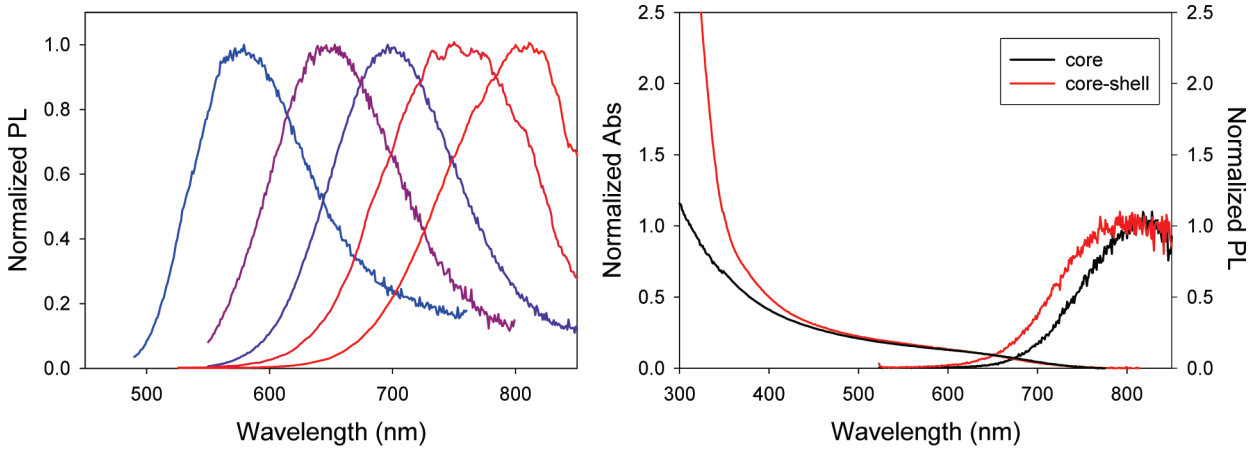

Figure 1. Left: PL spectra of $CuInS_2$ QDs (see Supporting Information for experimental details). Right: PL and absorbance spectra of $CuInS_2$ and $CuInS_2$/ZnS QDs.

obtained QDs provided poor QYs in the NIR region, and only one demonstration of *in vivo* imaging using these QDs has been recently reported.[27] In this report, we describe the synthesis of bright and photostable core/shell $CuInS_2$/ZnS QDs with emission ranging from the red to NIR using air-stable compounds. We show that these QDs could be easily transferred in water using two standard solubilization techniques and demonstrate their use for *in vivo* imaging of two regional LNs draining thoracic mammary fat pads in mice. We then compare the dose-dependent inflammatory response in the regional lymph nodes (LNs) induced by NIR CdTeSe/CdZnS and $CuInS_2$/ZnS functionalized with the same surface chemistry and show that $CuInS_2$/ZnS presents a much reduced toxicity compared to Cd-based QDs.

RESULTS AND DISCUSSION

QD Synthesis and Characterization. Synthesis of core $CuInS_2$ QDs is achieved in organic solvent at elevated temperatures. Typically, $InCl_3$ and CuCl salts are solubilized in octadecene in the presence of trioctylphosphine (TOP) and oleylamine. The sulfur precursor was injected at 190 °C in the form of bis(*N*-hexyldithiocarbamate) zinc, $Zn(NHDC)_2$, and the mixture was stirred at 190 °C for 10 min. We found that this precursor, formed from a primary amine, was more reactive and the obtained QDs were brighter than those obtained from other dithiocarbamate (*e.g.*, diethyldithiocarbamate, $Zn(DEDC)_2$) compounds as reported by Nakamura *et al.*[21] The resulting QDs are typically 3 ± 0.5 nm in diameter as measured by transmission electron microscopy (TEM, Figure S1 in Supporting Information). They display PL emission in the NIR, at around 800 nm, with typical QYs of 10−20% (Figure 1). Composition measurements confirm the presence of Cu, In, and S along with some incorporation of Zn. Consistently with previous reports, we found that the emission wavelengths of these QDs could be blue-shifted by varying the reaction time, temperature, or incorporating increasing amounts of Zn.[21] This provides, in particular, relatively bright near-infrared QDs (quantum yield ~ 10−20%) with a rapid and simple synthetic scheme, compared to previously reported syntheses.[26,27] However, these core-only QDs rapidly lose their PL when exposed to air or when transferred into water, which may be due to easy surface oxidation.

We therefore grew a ZnS shell around the $CuInS_2$ cores. The band offsets between these two materials allow for an efficient exciton confinement into the core and, therefore, should lead to increased PL QY and stability. We further note that the lattice mismatch between these materials is very small (~2%) and should allow growth of thick epitaxial shells without crystalline defects. Purified $CuInS_2$ cores were diluted in octadecene in the presence of excess oleic acid ligands. This solution was heated to 230 °C under inert atmosphere, and a solution of $Zn(NHDC)_2$ and zinc stearate in oleylamine and octadecene was injected dropwise in 30 min. The resulting QDs display a PL spectrum that is slightly blue-shifted compared to the core QDs (Figure 1), a feature that may be the sign of limited interdiffusion of Zn atoms into the $CuInS_2$ core and typical PL QY of 30%. Absorbance and PL excitation spectra reveal an increase in wavelength range below 350 nm, corresponding to contribution from the ZnS shell (Figure 1). Transmission electron microscopy (TEM) shows large monocrystalline nanocrystals of 5.5 ± 2 nm in diameter (Figure 2). Such thick ZnS shells can be grown without crystalline defects due to the very close lattice parameters of the two materials, in comparison with the CdSe/ZnS system in which only a few ZnS monolayers can be grown epitaxially. However, the current synthetic procedure leads to polydisperse shell thickness. X-ray diffraction of core and core/shell nanocrystals shows characteristic $CuInS_2$ (sphalerite) and ZnS (zinc blende) patterns (Figure S1, Supporting Information). Elemental analysis demonstrated the expected important increase in Zn composition due to growth of the ZnS shell (Figure S2 and Table S1, Supporting Information).

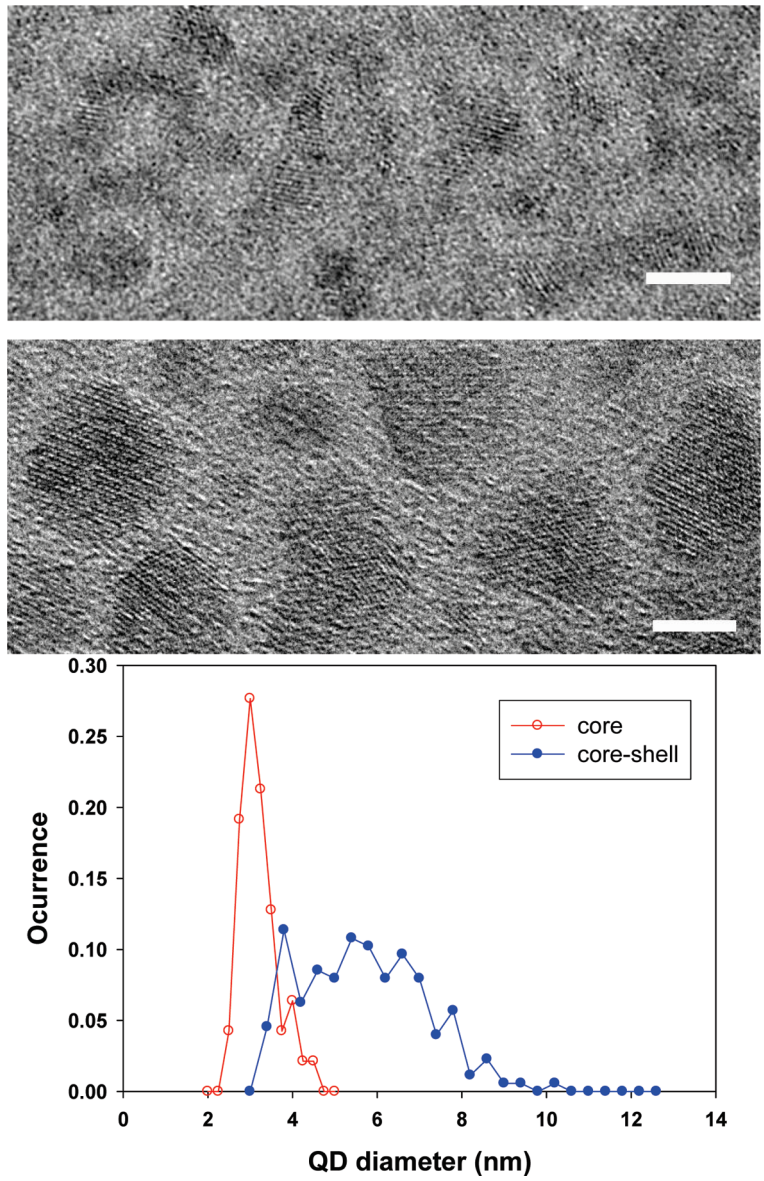

Figure 2. TEM image of $CuInS_2$ core (top panel) and $CuInS_2$/ZnS (middle panel) core/shell QDs. Scale bar: 5 nm. Bottom panel: Size distributions of core (open circles) and core−shell (filled circles) QDs as measured by TEM.

Water Solubilization. The resulting core−shell QDs could be successfully transferred into water using two of the most common water solubilization strategies, ligand exchange and phospholipid micelle encapsulation. The initial QDs are capped with hydrophobic ligands, either oleylamine or oleic acid or a mixture of both. These ligands could be exchanged with DHLA-PEG1000 (dihydrolipoic acid polyethylene glycol 1000) ligands.[28,29] Alternatively, the $CuInS_2$/ZnS QDs could be encapsulated into phospholipid micelles composed of DPPE-PEG2000 (dipalmitoyl phosphotidylethanolamine polyethyelene glycol 2000) terminated by methyl ether groups or including various percentages of other terminal functional groups (amines, carboxylic acid, *etc.*).[30,31] In both cases, the QDs display relatively high QYs after their transfer into water (~20%) and were stable for at least several weeks in water with negligible PL loss. In comparison, $CuInS_2$ core-only QDs only maintained a very weak PL QY after ligand exchange and transfer into water (<1%). In addition, we observed that our water-soluble $CuInS_2$/ZnS QDs displayed a much higher resistance to photobleaching than indocyanine green, a common NIR emitting organic dye (Figure S3, Supporting Information).

Regional Lymph Node Imaging. We then demonstrate for the first time utilization of these heavy-metal-free NIR QDs for *in vivo* imaging of the regional LNs. A solution of QDs encapsulated into phospholipid micelles composed of 33% PEG-COOH and 66% PEG-functionalized lipids in phosphate buffered saline (PBS) was prepared. The QD concentration was determined by measuring the In concentration by inductively coupled plasma mass spectroscopy (ICP-MS). A dose corresponding to 20 pmol of QDs was injected subcutaneously into the

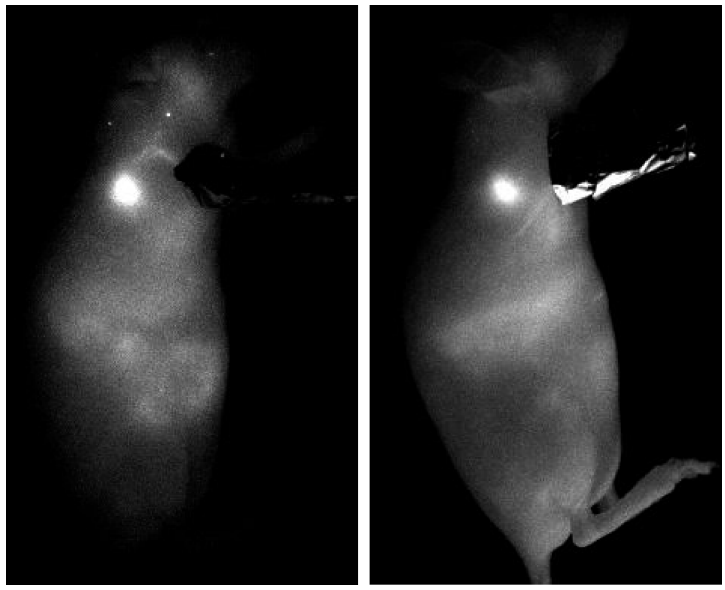

Figure 3. NIR fluorescence imaging of the RALN 15 min (left) and 7 days (right) after subcutaneous injection of 20 pmol micelle encapsulated QDs (66% DPPEPEG2000-Me/33% DPPEPEG2000-COOH) into the right anterior paw.

distal part of the right anterior paw of healthy mice. NIR fluorescence imaging was performed using a 690 nm laser excitation and a CCD camera with 10 ms integration time. The two regional LNs corresponding to right axillary LN (RALN) could be easily visualized as early as a few minutes after injection and for more than 7 days thanks to rapid QD migration and accumulation (Figure 3), similarly to what has been previously reported with CdTe-based QDs.[8,32,33] The right lateral thoracic LN (RLTLN) could also be visualized (Figure S4, Supporting Information). Similar images are obtained using QDs cap-exchanged with DHLAPEG1000 ligands (Figure S5). The ratio of RALN fluorescence signal over the autofluorescence at 24 h after injection is represented in Figure 4 as a function of the injected QD quantity. The signal detected is directly proportional to the injected dose, and we estimate that the limit of detectability corresponds to a 2 pmol injected dose, for which the signal (S) to autofluorescence background (B) ratio is over $B + 3\sigma$, where σ is the average pixel-to-pixel standard deviation.

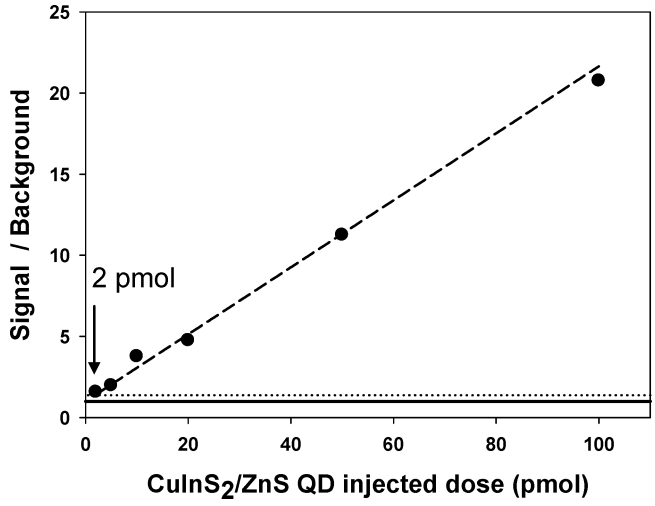

Figure 4. Ratio of the RALN NIR fluorescence signal at 24 h post-injection *vs* autofluorescence background plotted as a function of the $CuInS_2$/ZnS QD injected dose (dashed line is the corresponding linear regression). The solid line represents the autofluorescence background, and the dotted line represents the autofluorescence background plus three times the pixel-to-pixel standard deviation.

QD-Induced Lymph Node Inflammation. We have shown in a previous study of regional LN imaging using QDs that QDs injected subcutaneously accumulated preferentially at the injection point and in the two regional LNs with concentrations typically at least 10 times higher than in other organs, even after more than a week post-injection.[33] It is therefore likely that these organs will be more sensitive toward acute QD toxicity. Indeed, we observed that injection of 20 pmol of CdTeSe/CdZnS QDs in the right anterior paw induced an immune response revealed by an inflammation of the two regional LNs. This inflammation is a reflection of the acute local toxicity of CdTeSe/CdZnS QDs and represents a serious obstacle to potential clinical applications, even though no signs of abnormal motivity behavior were noticed and no signs of dehydratation were registered in injected mice.[33] We attributed this toxicity to the degradation of the QDs *in vivo* and the release of toxic heavy metal ions such as Cd and Te, in agreement with previous studies of QD toxicity.[9,16] Here we compare the acute toxicity of CdTeSe/CdZnS and $CuInS_2$/ZnS QDs used for regional LN imaging. We note that both QD batches display similar imaging performance due to similar extinction coefficients at our excitation wavelength ($\sim 5-6 \times 10^5$ M^{-1} cm^{-1} at 690 nm for these $CuInS_2$/ZnS and CdTeSe/CdZnS QD batches), quantum yields ($\sim$20−30%), and hydrodynamic sizes ($\sim$20−22 nm)).

Both QD batches were encapsulated in functionalized phospholipid micelles (33% PEG2000-COOH; 66% PEG2000) and purified by ultracentrifugation (see Materials and Methods section). Twenty microliters of QD solution prepared with various dilutions were injected subcutaneously in the right anterior paw of mice. The weights of the RALN and RLTLN dissected 7 days after injection are reported in Figure 5 for both QD batches and compared to controls (mice injected with the same volume of saline solution). The QD concentration in the LNs was proportional to the quantity injected as indicated by elemental ICP-MS analysis, meaning that there was no saturation in QD uptake in the concentration range studied here. The percentage of the total injected dose (% ID) captured by the RALN after 7 days is slightly larger for $CuInS_2$/ZnS QDs (typically 4% ID; see Figure S6, Supporting Information) than for CdTeSe/CdZnS (typically 1.5% ID; see ref 33). We note for both QD batches a clear dose-dependent increase in weight

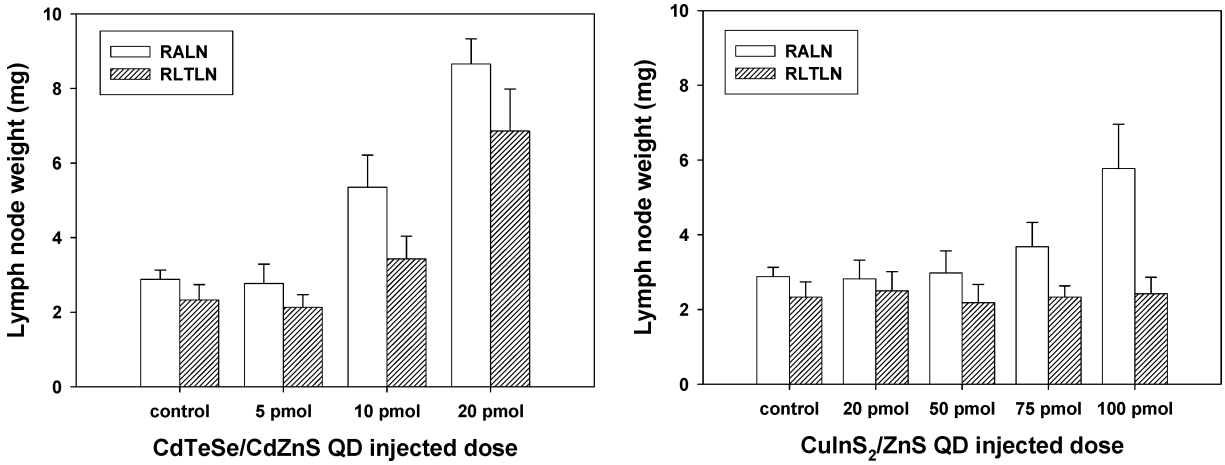

Figure 5. Weight of the RALN and RLTLN dissected 7 days post-injection as a function of the QD injected dose for CdTeSe/CdZnS (left panel) and $CuInS_2$/ZnS (right panel) QDs. The data are mean ± SEM (n = 6 per group).

of the RALNs, reflecting the increasing toxicity of the QDs. However, there is a clear difference in toxicity between the two batches. An inflammation is already clearly noticed for 10 pmol of injected CdTeSe/CdZnS QDs with a significant increase of RALN weight (average RALN weight 5.35 ± 0.86 mg *vs* 2.88 ± 0.25 mg for controls; $p < 0.01$). In contrast, the same level of inflammation is reached for an injection of 100 pmol of $CuInS_2$/ZnS (average RALN weight 5.77 ± 1.19 mg; $p < 0.01$). The same influence of QD composition is observed in the RLTLN, another regional LN capturing typically 1% ID; no significant inflammation is observed in this LN for injections of up to 100 pmol of $CuInS_2$/ZnS, while an injection of 10 pmol of CdTeSe/CdZnS induces a significant increase in RLTLN weight compared to control (3.43 ± 0.61 mg *vs* 2.33 ± 0.41 mg; $p < 0.05$). Histological sections of RALNs dissected 7 days post-injection are presented in Figure 6. The RALN of mice injected with 20 pmol of $CuInS_2$/ZnS showed no appreciable difference with control LNs, whereas the RALN of mice injected with the same dose of CdTeSe/CdZnS QDs clearly showed inflammation sites (light areas). These signs of inflammation included numerous polynuclears, some histiocytes, and vacuoles of digestion in studied areas (data not shown).

Several studies have shown that acute CdSe QD toxicity in cell cultures originated mainly from release of Cd^{2+} ions and depended on many factors including QD size, presence of inorganic shell, and nature of the organic capping layer.[9−16] In contrast, there has been much less studies of *in vivo* QD toxicity. The majority of studies showed an accumulation of injected QD into reticuloendothelial system organs (liver, spleen, LNs) over long periods (several months or years) without elimination,[17−19,34] except for small QDs coated with specific surface chemistry.[35] This long-term sequestration will eventually lead to the degradation of the organic capping layer and to a slow release of the QD inorganic material.[34] The clear difference in toxicity between $CuInS_2$/ZnS and CdTeSe/CdZnS observed in our work indicates that some of the inorganic material may also be released on short time scales (a few days). Even with more robust surface chemistries able to slow the release of metal ions, concentrations of Cd^{2+} ions are likely to eventually build up in targeted organs given the long metabolic lifetime of QDs and Cd^{2+} ions.[34] Clinical applications will therefore require QDs that do not contain toxic heavy metal.

Overall, $CuInS_2$ QDs display many advantages over other semiconductor nanocrystals, such as, for example, II−VI, IV−VI, or III−V semiconductors, in that they provide QDs emitting in the visible and NIR range without toxic elements and can be efficiently protected from oxidation by thick ZnS shells thanks to similar lattice parameters. Optimization of the synthetic procedures for core and shell growth should further improve the optical and structural quality of these nanocrystals (monodispersity of the core and core−shell QD populations, improved PL QY). $CuInS_2$/ZnS nanocrystals appear to present a much reduced *in vivo* local acute toxicity com-

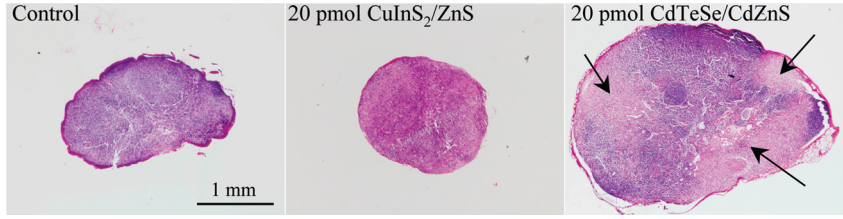

Figure 6. Histological sections of the RALNs resected 7 days post-injection for mice injected with a saline buffer solution (control), 20 pmol of $CuInS_2$/ZnS QDs, and 20 pmol of CdTeSe/CdZnS QDs. The black arrows indicate inflammation sites (light areas). The scale bar corresponds to 1 mm.

pared to CdTeSe/CdZnS QDs. Interestingly, we note that the minimal dose of $CuInS_2$/ZnS QDs required to detect the RALN (2 pmol) is about 50 times smaller than the onset of RALN inflammation. Further work will be needed to study long-term toxicity effects after several months or several years post-injection, but we expect that $CuInS_2$/ZnS will be confirmed as a much less toxic alternative to II−VI or IV−VI materials and will find many applications for *in vivo* biomedical imaging where toxic heavy metals cannot be tolerated.

MATERIALS AND METHODS

All chemicals were purchased from Sigma-Aldrich and used without further purification, unless indicated otherwise.

QD Synthesis. Bis(*N*-hexyldithiocarbamate) zinc ($Zn(NHDC)_2$) was prepared according to previously reported procedures.[36] To obtain core QDs emitting at around 800 nm, 0.2 mmol of CuCl, 0.2 mmol of $InCl_3$, 2 mL of trioctylphosphine (TOP), 2 mL of oleylamine, and 10 mL of octadecene (ODE) were mixed in a three-neck flask and degassed under vacuum at 70 °C for 20 min. This solution was then placed under argon atmosphere and heated to 190 °C. A solution of 0.2 mmol of $Zn(NHDC)_2$ dispersed in 1 mL of TOP was swiftly injected into the flask. The mixture was kept at 190 °C for 10 min and then cooled to room temperature. These core nanocrystals were purified by precipitation in ethanol and acetone and resuspended in 9 mL of hexane and 1 mL of TOP. QDs with different emission wavelengths could be obtained by adding different amount of $ZnCl_2$ (0.2−1 mmol) along with the Cu and In salts.

QDs emitting at bluer wavelengths were synthesized by the same procedures with slight modifications. Examples of PL spectra for different QDs are shown in the left panel of Figure 1. These QDs were synthesized using the following modifications of the above procedure: (i) 0.1 mmol of CuCl; 0.1 mmol of $InCl_3$, and 0.6 mmol of $ZnCl_2$ in the flask before injection (emission ~580 nm); (ii) 0.2 mmol of CuCl, 0.2 mmol of $InCl_3$, and 0.5 mmol of $ZnCl_2$ in the flask before injection, 2 min growth time (emission ~650 nm); (iii) 0.2 mmol of CuCl, 0.2 mmol of $InCl_3$, and 0.5 mmol of $ZnCl_2$ in the flask before injection 10 min growth time (emission ~700 nm); (iv) 0.2 mmol of CuCl, 0.2 mmol of $InCl_3$, no $ZnCl_2$. The reaction temperature was set to 170 °C instead of 190 °C (emission ~750 nm).

Growth of the ZnS shell was performed as follows: 2 mL of core QD solution prepared as described above was mixed with 10 mL of ODE and 2 mL of oleic acid. The solution was degassed under vacuum at 70 °C for 30 min then heated at 230 °C under argon. A solution of 0.2 mmol $Zn(NHDC)_2$ and 0.6 mmol zinc stearate in 1 mL of TOP, 1 mL of oleylamine, and 8 mL of ODE was injected dropwise in 20 min. The resulting QDs were then purified after cooling by precipitation in ethanol and acetone and resuspended in hexane.

CdTeSe/CdZnS QDs were synthesized following previously published protocols.[37] The resulting QDs were emitting at 800 nm with a CdZnS shell thickness of typically ~1−1.5 nm.

QD Characterization. Photoluminescence and photoluminescence excitation spectra were acquired using a Fluoromax-3 fluorimeter (Jobin Yvon, Horiba). Photoluminescence quantum yields were measured using indocyanine green (ICG) as a standard (13% in DMSO). Optical densities (OD) of QD and dye standard solutions were measured using a Cary-5E UV−vis spectrophotometer (Varian, Les Ulis, France), and the QYs were obtained following

$$QY_{QD} = QY_{dye}\frac{OD_{dye}}{OD_{QD}}\frac{{n_{QD}}^2}{{n_{dye}}^2}$$

Transmission electron microscopy (TEM) images were acquired on a JEOL 2010 field electron gun microscope. Elemental analysis was performed by energy-dispersive X-ray spectroscopy (EDS) on a Hitachi S-3600N scanning electron microscope. X-ray diffraction patterns were acquired using a Philips X'Pert diffractometer with a Cu Kα source.

QD Solubilization in Water. The core/shell QDs could be transferred into water either by ligand exchange with dihydrolipoic acid/polyethylene glycol 1000 (DHLAPEG1000) or by micelle encapsulation: DHLAPEG1000 ligands were prepared according to previously published protocols.[28] One hundred microliters of as-prepared core−shell QDs was precipitated in ethanol and resuspended in 300 μL of chloroform and 100 mg of DHLAPEG1000. The solution was kept at 60 °C overnight. The QDs were then precipitated in an ethanol/hexane mixture, resuspended in water, and purified by membrane ultrafiltration (2 cycles of centrifugation in Vivaspin 10 kDa, Sartorius).

Micelle encapsulation was performed according to previously published protocols.[30,31] Typically, 100 μL of core/shell nanocrystals prepared as indicated above was washed with two cycles of precipitation in ethanol and resuspension in hexane and finally resuspended in 100 μL of choloroform. The QDs were then mixed with 200 μL of DPPE-PEG2000-Me (dipalmitoyl phosphotidylethanolamine polyethyelene glycol 2000 methyl ether, Novalyst, France) phospholipid solution at 20 mg/mL in chloroform, 200 μL of DPPE-PEG2000-COOH (Novalyst, France) at 10 mg/mL, and 1 mL of deionized water. The chloroform was evaporated by heating at 80 °C, yielding a limpid solution. These water-soluble QDs were then purified by ultracentrifugation following previously published protocols.[30,31]

Animals. Ten to 12 week old female balb/c mice (Balb/cOlaHsd) (Harlan, Gannat, France) weighing from 18 to 22 g were used in these experiments. Mice were kept in 12 h light/dark cycle and had access to food and water *ad libitum*. The mice were acclimated for 2 weeks prior to use. Specific purified diet (TD.94045, Harlan Teklad, Madison, WI) was used to reduce tissue autofluorescence in the NIR spectral region. The animals received care in accordance with established guidelines of FELASA (Federation of European Laboratory Animal Science Associations), and animal procedures were performed in compliance with institutional and national guidelines. All experiments were performed under anesthesia using intraperitoneal injection of 0.01 mL/g of body weight of a solution containing 9 mg/mL of ketamine (Ketalar, Panpharma, Fougères, France) and 0.9 mg/mL of xylazine (Rompun, Bayer Pharma, Puteaux, France).

QD Administration. Control mice were injected subcutaneously in the distal part of the right anterior paw with 20 μL of PBS, and for experimental groups, 20 μL of different solutions of CdTeSe/CdZnS QD (1, 0.5, and 0.25 μM corresponding to 20, 10, and 5 pmol, respectively) and $CuInS_2$/ZnS QD (5, 3.75, 2.5, 1, 0.5, 0.25, 0.1, and 0.05 μM corresponding to 100, 75, 50, 20, 10, 5, 2, and 1 pmol, respectively) was administrated by the same way. After product delivery, the right paw was kneaded to improve product migration.

***In Vivo* Near-Infrared Fluorescence Imaging.** *In vivo* optical imaging of QDs was performed using a Fluobeam 700 NIR imaging system (Fluoptics, Grenoble, France). The power density of laser irradiation on tissue was 7 mW/cm^2. The regions of interest (ROIs) were depilated using a commercial hair-removal cream before imaging. The CCD camera shows the specificity to adjust the fluorescence signal on the pixel which presents the strongest fluorescence intensity. Thus, the injection point of QDs was hidden, allowing a better ROIs visualization.

Detection Limit of $CuInS_2$/ZnS QDs in Regional Lymph Nodes. Mice were injected subcutaneously with 10, 5, 2, and 1 pmol of $CuInS_2$/ZnS QD (n = 1 per group). *In vivo* fluorescence of RALNs and RLTLNs was recorded at 5 and 60 min at 24 h and 7 days post-injection.

Inductively Coupled Plasma Mass Spectroscopy (ICP-MS). A Varian 820 MS instrument (Varian, Les Ulis, France) was used for quantification of QD concentration in organs and in solution by ICP-MS. All biological samples were completely dissolved with 70% HNO_3 and heated at 90 °C until total mineralization. Each mineralized sample was solubilized in 25 mL of Milli-Q water (resistivity >18.2

MΩ) and analyzed by ICP-MS at the Laboratoire Environnement-Hygiène of ASCAL (Forbach, France). The ICP-MS instrument was initialized, optimized, and standardized using the manufacturer's recommendations. The limit of indium quantification was 50 ng/mL. Five samples of 1 mL of $CuInS_2$/ZnS QD solutions at 20 nM (20 pmol) have been analyzed in the same conditions, previously described, to correlate indium and QD concentrations. After fluorescence imaging of mice for up to 7 days and their sacrifice by cervical dislocation, four groups of animals ($n = 3$ per group) were used to quantify indium in the two regional LNs after their resection: three experimental groups were injected with 100, 50, and 20 pmol of QDs, and one control group received PBS. All removed samples were weighed and stored at −80 °C prior to elemental analysis. All data are represented as mean ± SD (standard deviation).

Histology of Lymph Nodes Section. Mice received CdTeSe/CdZnS QDs (20, 10, and 5 pmol) and $CuInS_2$/ZnS QDs (100, 75, 50, and 20 pmol) and were sacrificed 7 days post-injection ($n = 6$ per group for CdTeSe/CdZnS QDs and $n = 3$ for $CuInS_2$/ZnS QDs). RALNs and RLTLNs were removed and weighed for histological analysis. All tissues were fixed in 10% formaldehyde, 5 μm sections of LNs were prepared, and hematoxylin and eosin (H&E) staining was performed and examined to visualize inflammatory changes.

Acknowledgment. We thank M. Hanafi for help with elemental analysis, X. Xu and P. Bassoul for help with TEM imaging, and A. Leroux for histological analysis.

Supporting Information Available: XRD patterns, elemental analysis, additional NIR imaging, lymph node uptake quantification, EDX analysis, X-ray diffraction, photostability, additional NIR fluorescence imaging, quantification of $CuInS_2$/ZnS QD % ID in the regional LNs. This material is available free of charge *via* the Internet at http://pubs.acs.org.

REFERENCES AND NOTES

1. Efros, A. L.; Rosen, M. The Electronic Structure of Semiconductor Nanocrystals. *Annu. Rev. Mater. Sci.* **2000**, *30*, 475–521.
2. Murray, C. B.; Kagan, C. R.; Bawendi, M. G. Synthesis and Characterization of Monodisperse Nanocrystals and Close-Packed Nanocrystal Assemblies. *Annu. Rev. Mater. Sci.* **2000**, *30*, 545–610.
3. Medintz, I. L.; Uyeda, H. T.; Goldman, E. R.; Mattoussi, H. Quantum Dot Bioconjugates for Imaging, Labelling and Sensing. *Nat. Mater.* **2005**, *4*, 435–446.
4. Michalet, X.; Pinaud, F. F.; Bentolila, L. A.; Tsay, J. M.; Doose, S.; Li, J. J.; Sundaresan, G.; Wu, A. M.; Gambhir, S. S.; Weiss, S. Quantum Dots for Live Cells, *In Vivo* Imaging, and Diagnostics. *Science* **2005**, *307*, 538–544.
5. Gao, X. H.; Cui, Y. Y.; Levenson, R. M.; Chung, L. W. K.; Nie, S. M. *In Vivo* Cancer Targeting and Imaging with Semiconductor Quantum Dots. *Nat. Biotechnol.* **2004**, *22*, 969–976.
6. Voura, E. B.; Jaiswal, J. K.; Mattoussi, H.; Simon, S. M. Tracking Metastatic Tumor Cell Extravasation with Quantum Dot Nanocrystals and Fluorescence Emission-Scanning Microscopy. *Nat. Med.* **2004**, *10*, 993–998.
7. Frangioni, J. V.; Kim, S. W.; Ohnishi, S.; Kim, S.; Bawendi, M. G. Sentinel Lymph Node Mapping with Type-II Quantum Dots. *Methods Mol. Biol.* **2007**, *374*, 147–159.
8. Kim, S.; Lim, Y. T.; Soltesz, E. G.; De Grand, A. M.; Lee, J.; Nakayama, A.; Parker, J. A.; Mihaljevic, T.; Laurence, R. G.; Dor, D. M.; Cohn, L. H.; Bawendi, M. G.; Frangioni, J. V. Near-Infrared Fluorescent Type II Quantum Dots for Sentinel Lymph Node Mapping. *Nat. Biotechnol.* **2004**, *22*, 93–97.
9. Derfus, A. M.; Chan, W. C. W.; Bhatia, S. N. Probing the Cytotoxicity of Semiconductor Quantum Dots. *Nano Lett.* **2004**, *4*, 11–18.
10. Hoshino, A.; Fujioka, K.; Oku, T.; Suga, M.; Sasaki, Y. F.; Ohta, T.; Yasuhara, M.; Suzuki, K.; Yamamoto, K. Physicochemical Properties and Cellular Toxicity of Nanocrystal Quantum Dots Depend on Their Surface Modification. *Nano Lett.* **2004**, *4*, 2163–2169.
11. Kirchner, C.; Liedl, T.; Kudera, S.; Pellegrino, T.; Javier, A. M.; Gaub, H. E.; Stolzle, S.; Fertig, N.; Parak, W. J. Cytotoxicity of Colloidal CdSe and CdSe/ZnS Nanoparticles. *Nano Lett.* **2005**, *5*, 331–338.
12. Oberdorster, G.; Oberdorster, E.; Oberdorster, J. Nanotoxicology: An Emerging Discipline Evolving from Studies of Ultrafine Particles. *Environ. Health Persp.* **2005**, *113*, 823–839.
13. Hardman, R. A Toxicologic Review of Quantum Dots: Toxicity Depends on Physicochemical and Environmental Factors. *Environ. Health Persp.* **2006**, *114*, 165–172.
14. Cho, S. J.; Maysinger, D.; Jain, M.; Roder, B.; Hackbarth, S.; Winnik, F. M. Long-Term Exposure to CdTe Quantum Dots Causes Functional Impairments in Live Cells. *Langmuir* **2007**, *23*, 1974–1980.
15. Smith, A. M.; Duan, H. W.; Mohs, A. M.; Nie, S. M. Bioconjugated Quantum Dots for *In Vivo* Molecular and Cellular Imaging. *Adv. Drug Delivery Rev.* **2008**, *60*, 1226–1240.
16. Lewinski, N.; Colvin, V.; Drezek, R. Cytotoxicity of Nanoparticles. *Small* **2008**, *4*, 26–49.
17. Ballou, B.; Lagerholm, B. C.; Ernst, L. A.; Bruchez, M. P.; Waggoner, A. S. Noninvasive Imaging of Quantum Dots in Mice. *Bioconjugate Chem.* **2004**, *15*, 79–86.
18. Fischer, H. C.; Liu, L. C.; Pang, K. S.; Chan, W. C. W. Pharmacokinetics of Nanoscale Quantum Dots: *In Vivo* Distribution, Sequestration, and Clearance in the Rat. *Adv. Funct. Mater.* **2006**, *16*, 1299–1305.
19. Duconge, F.; Pons, T.; Pestourie, C.; Herin, L.; Theze, B.; Gombert, K.; Mahler, B.; Hinnen, F.; Kuhnast, B.; Dolle, F.; Dubertret, B.; Tavitian, B. Fluorine-18-Labeled Phospholipid Quantum Dot Micelles for *In Vivo* Multimodal Imaging from Whole Body to Cellular Scales. *Bioconjugate Chem.* **2008**, *19*, 1921–1926.
20. Castro, S. L.; Bailey, S. G.; Raffaelle, R. P.; Banger, K. K.; Hepp, A. F. Nanocrystalline Chalcopyrite Materials ($CuInS_2$ and $CuInSe_2$) *via* Low-Temperature Pyrolysis of Molecular Single-Source Precursors. *Chem. Mater.* **2003**, *15*, 3142–3147.
21. Nakamura, H.; Kato, W.; Uehara, M.; Nose, K.; Omata, T.; Otsuka-Yao-Matsuo, S.; Miyazaki, M.; Maeda, H. Tunable Photoluminescence Wavelength of Chalcopyrite $CuInS_2$-Based Semiconductor Nanocrystals Synthesized in a Colloidal System. *Chem. Mater.* **2006**, *18*, 3330–3335.
22. Torimoto, T.; Adachi, T.; Okazaki, K.; Sakuraoka, M.; Shibayama, T.; Ohtani, B.; Kudo, A.; Kuwabata, S. Facile Synthesis of ZnS-$AgInS_2$ Solid Solution Nanoparticles for a Color-Adjustable Luminophore. *J. Am. Chem. Soc.* **2007**, *129*, 12388–12389.
23. Panthani, M. G.; Akhavan, V.; Goodfellow, B.; Schmidtke, J. P.; Dunn, L.; Dodabalapur, A.; Barbara, P. F.; Korgel, B. A. Synthesis of $CuInS_2$, $CuInSe_2$, and $Cu(InXGa_{1-x})Se_2$ (CIGS) Nanocrystal "Inks" For Printable Photovoltaics. *J. Am. Chem. Soc.* **2008**, *130*, 16770–16777.
24. Allen, P. M.; Bawendi, M. G. Ternary I−III−VI Quantum Dots Luminescent in the Red to Near-Infrared. *J. Am. Chem. Soc.* **2008**, *130*, 9240–9241.
25. Koo, B.; Patel, R. N.; Korgel, B. A. Synthesis of $CuInSe_2$ Nanocrystals with Trigonal Pyramidal Shape. *J. Am. Chem. Soc.* **2009**, *131*, 3134–3135.
26. Xie, R.; Rutherford, M.; Peng, X. Formation of High-Quality I−III−VI Semiconductor Nanocrystals by Tuning Relative Reactivity of Cationic Precursors. *J. Am. Chem. Soc.* **2009**, *131*, 5691–5697.
27. Li, L.; Daou, T. J.; Texier, I.; Tran, T. K. C.; Nguyen, Q. L.; Reiss, P. Highly Luminescent $CuInS_2$/ZnS Core/Shell Nanocrystals: Cadmium-Free Quantum Dots for *In Vivo* Imaging. *Chem. Mater.* **2009**, *21*, 2422–2429.
28. Uyeda, H. T.; Medintz, I. L.; Jaiswal, J. K.; Simon, S. M.; Mattoussi, H. Synthesis of Compact Multidentate Ligands to Prepare Stable Hydrophilic Quantum Dot Fluorophores. *J. Am. Chem. Soc.* **2005**, *127*, 3870–3878.

29. Susumu, K.; Uyeda, H. T.; Medintz, I. L.; Pons, T.; Delehanty, J. B.; Mattoussi, H. Enhancing the Stability and Biological Functionalities of Quantum Dots *via* Compact Multifunctional Ligands. *J. Am. Chem. Soc.* **2007**, *129*, 13987–13996.
30. Dubertret, B.; Skourides, P.; Norris, D. J.; Noireaux, V.; Brivanlou, A. H.; Libchaber, A. *In Vivo* Imaging of Quantum Dots Encapsulated in Phospholipid Micelles. *Science* **2002**, *298*, 1759–1762.
31. Carion, O.; Mahler, B.; Pons, T.; Dubertret, B. Synthesis, Encapsulation, Purification and Coupling of Single Quantum Dots in Phospholipid Micelles for Their Use in *In Vivo* Imaging. *Nat. Protoc.* **2007**, *2*, 2383–2390.
32. Ballou, B.; Ernst, L. A.; Andreko, S.; Harper, T.; Fitzpatrick, J. A. J.; Waggoner, A. S.; Bruchez, M. P. Sentinel Lymph Node Imaging Using Quantum Dots in Mouse Tumor Models. *Bioconjugate Chem.* **2007**, *18*, 389–396.
33. Pic, E.; Pons, T.; Bezdetnaya, L.; Leroux, A.; Guillemin, F.; Dubertret, B.; Marchal, F. Fluorescence Imaging and Whole-Body Biodistribution of Near-Infrared Emitting Quantum Dots after Subcutaneous Injection for Regional Lymph Node Mapping in Mice. *Mol. Imaging Biol.* doi: 10.1007/s11307-009-0288-y.
34. Fitzpatrick, J. A. J.; Andreko, S. K.; Ernst, L. A.; Waggoner, A. S.; Ballou, B.; Bruchez, M. P. Long-Term Persistence and Spectral Blue Shifting of Quantum Dots *In Vivo*. *Nano Lett.* **2009**, *9*, 2736–2741.
35. Choi, H. S.; Liu, W.; Misra, P.; Tanaka, E.; Zimmer, J. P.; Ipe, B. I.; Bawendi, M. G.; Frangioni, J. V. Renal Clearance of Quantum Dots. *Nat. Biotechnol.* **2007**, *25*, 1165–1170.
36. Memon, A. A.; Afzaal, M.; Malik, M. A.; Nguyen, C. Q.; O'Brien, P.; Raftery, J. The *N*-Alkyldithiocarbamato Complexes $[M(S_2CNHR)_2]$ (M = Cd(II) Zn(II); R = C_2H_5, C_4H_9, C_6H_{13}, $C_{12}H_{25}$); Their Synthesis, Thermal Decomposition and Use To Prepare of Nanoparticles and Nanorods of CdS. *Dalton Trans.* **2006**, 4499–4505.
37. Pons, T.; Lequeux, N.; Mahler, B.; Sasnouski, S.; Fragola, A.; Dubertret, B. Synthesis of Near-Infrared-Emitting, Water-Soluble CdTeSe/CdZnS Core/Shell Quantum Dots. *Chem. Mater.* **2009**, *21*, 1418–1424.